

# GEO Satellite Characterization through Polarimetry using Simultaneous Observations from nearby Optical Sensors

Manuel Cegarra Polo, Andrey Alenin, Israel Vaughn and Andrew Lambert  
*School of Engineering and IT, UNSW Canberra, Canberra, Australia*

## ABSTRACT

Polarimetry has shown capacity for both geometry inference and material classification in recent years. By carefully selecting a polarimetric modality with higher contrast for the objects of interest, it becomes possible to discriminate those objects by leveraging the understanding of differing geometry, material characteristics, and its mapping into consequent polarisation measurements. Expansion of the measurement dimensionality increases the potential to discriminate unresolved objects, thereby widening the possible set of imaging tasks. The use of polarimetry as a technique to characterise non-resolved GEO satellites using telescopes of small aperture (less than 0.5 meters) is currently under study by the Space Research Group in UNSW Canberra. First experiments are currently being performed in order to evaluate the use of this technique to characterise GEO satellites. A comparison of both polarimetric and irradiance only acquisitions is being implemented.

Two telescopes separated by 1000m are used for the experiments. One of them (USAF funded Falcon Telescope Network) has the capability to be remote controlled and time tasks assigned, and the other can be operated on-site and is connected to a computer in a network which can control the former with known latency, both synchronised by the same GPS clock. A linear polariser is situated in a collimated beam section of the light path in one of the telescopes to capture polarised photometric measurements, while the other is acquiring the non-polarised photometric signature of the same GEO satellite under observation. The telescope detectors are to be radiometrically calibrated to one another in order to evaluate the photometric data at the same scale.

We evaluate the polarised and non-polarised synchronous time photometric curves as a preliminary test to determine satellite signature and its variation over time. We report on the discrimination of unresolved satellites and the merit of including polarisation sensing within the task.

## 1. INTRODUCTION

Geostationary satellites are located at a distance where they cannot be resolved, even by current large aperture ground telescopes. To estimate the ground resolution  $R$  of a telescope [1] in order to image RSO (Resident Space Objects) we can use the expression:

$$R = 2.44 h \lambda / D,$$

where  $h$  is the slant range,  $\lambda$  the wavelength and  $D$  the telescope aperture diameter.

From the previous expression, table 1 shows the diffraction limited ground resolution for different diameters of a telescope when imaging objects in the visible spectrum ( $\lambda = 0.5 \mu\text{m}$  was considered for this calculation) in the geosynchronous belt, at an approximate height of 36 000 km.

Table 1. Lineal resolution limited by diffraction of various telescopes apertures.

Telescope Diameter (m)	Ground Resolution (m)
0.3	146.4
0.5	87.84
1	43.92
3	14.64
5	8.78
8	5.49
10	4.39

With a 10 meter aperture telescope, we could obtain a theoretical diffraction limited resolution of 4.39 meters. Atmospheric turbulence will degrade the imaging quality further. To diminish the effect of the turbulence aberration in the images techniques such as adaptive optics can be used, and some researchers have explored this path [2].

A different technique used to obtain resolved images from geostationary satellites is interferometry, and several researchers have investigated its possible implementation, through simulations and preliminary studies [3,4].

Big telescope facilities are expensive to maintain and operate, and usually provide particular time slots for researchers, with costly sessions, which are not always productive due to weather factors. In contrast, access to small telescopes (less than 1 meter) by the research community is better facilitated since they are more affordable, they are normally close to the university or research center or in mobile platforms and there are often more chances to obtain results in case of bad weather nights due to lower demand over large telescopes.

An adequate characterization of geosynchronous satellites through reflected light from the Sun requires a comprehensive set of observations during an extended number of nights, due to the different phase angles of the satellite during the year and other variations in satellite attitude and observation angles. The availability of close, accessible and affordable telescope facilities ease this process and the use of small telescopes can facilitate a long term study of geostationary satellites. At UNSW Canberra, telescope facilities include one node of the Falcon Telescope Network (FTN) and a couple of high end amateur telescopes (a 0.4 meters Meade LX200ACF and a 0.3 meters Meade LX200EMC).

Techniques used to study unresolved optical signatures from passively sun-lit satellites are intensity/radiance measurements, spectral measurements, and polarimetric measurements. Obtaining the light curves through intensity measurements has been used for many years now, with successful results when detecting tumbling or faulty satellites [5,6]. Spectra from intensity measurements is a more recent technique with promising results, although results should be carefully interpreted [7].

As some authors stated [8], the use of polarisation information is an underused technique, and in the particular case of the reflected light from geostationary satellites we found that it is indeed a not very well explored path by the research community. There are simulation [9], laboratory results [10], and some on-sky experimental results [11,12]. Classification using polarimetric techniques has shown promise in non-astronomical applications [13,14], with utility recently being shown via active polarimetry for unresolved images [13].

We intend to evaluate experimentally passive polarisation as a technique to extract information from geostationary satellites, not available through intensity or spectra measurements, with possible applications to satellite identification, attitude detection, characterization and aging of materials of in-orbit satellites. High fidelity characterization techniques for unresolved satellites, however, will likely require a fusion of spectral, polarimetric, and intensity/radiance techniques.

## **2. TELESCOPES ARRANGEMENT AND POLARISATION OPTO-MECHANICAL SETUP**

Two telescopes separated a distance of 1 km were used to perform the experiments. One telescope (FTN Canberra node 0.5m) captures the intensity only measurements, and the other (LX200EMC 0.3m) has a linear polarizer mounted in a rotator stage installed to obtain different angles of polarisation. Both telescopes acquire images in a synchronous way and have their cameras calibrated in a simple way (discussed below) in this preliminary communication. Fig. 1 shows this setup.

FTN (Falcon Telescope Network) Canberra node is a 0.5 m diameter telescope that can be accessed remotely and can work in an automated mode. The other telescope is a 0.3 meter Meade LX200 EMC, located on the roof of building 16 on UNSW Canberra Campus. A computer connected locally to the 0.3 meter telescope includes software developed in-house to control local peripheral (camera and rotator) and remote Falcon facilities.

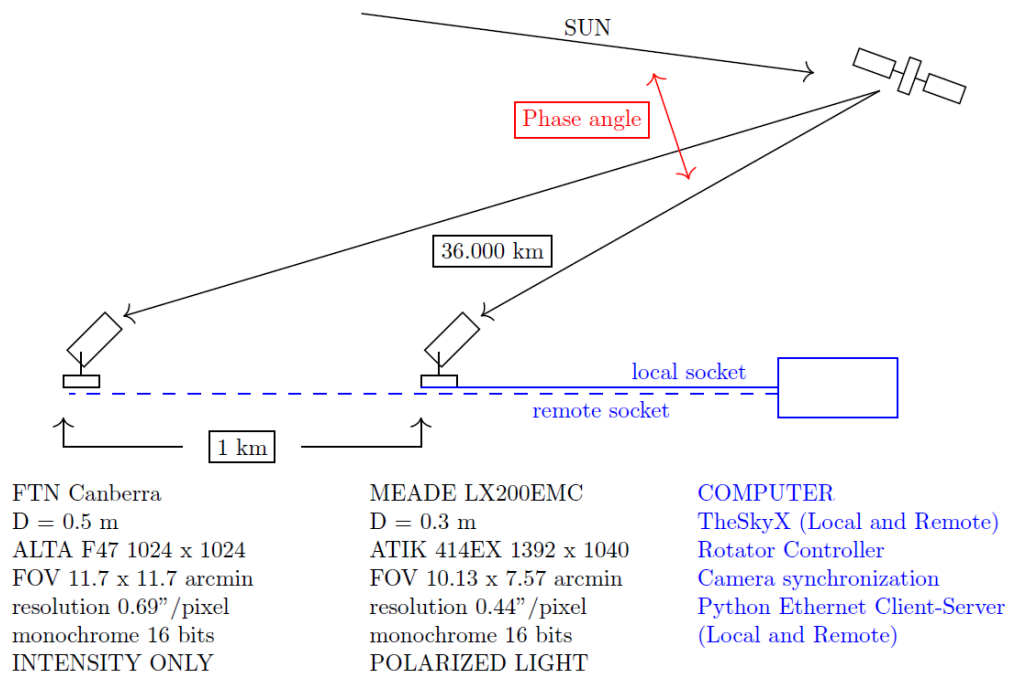


Fig. 1. Telescopes arrangement.

Fig. 2 (left) shows the polarimetric system consisting of a programmable rotation stage attached to the optical train and the science camera. The optical train consists of a negative lens which creates a collimated beam entering the linear polarizer, followed by a positive lens to refocus the image in the science camera.

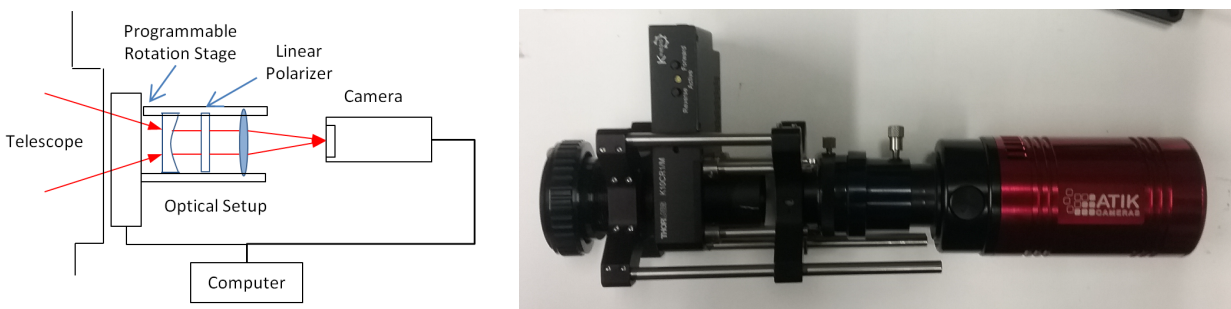


Fig. 2. (Left) Opto-mechanical setup, (Right) picture of the opto-mechanical system.

### 3. CALIBRATION OF CAMERAS

Since we are using two different telescopes with different cameras, a proper calibration of both optical systems is required. Table 2 shows a list of all important features of both telescopes and their cameras.

Table 2. Main characteristics of telescopes and their cameras

Telescope	FTN Officina Stellare	Meade LX200 EMC
Diameter	0.5 m	0.3 m
Mount	Equatorial	Equatorial
F number	F/8	F/10
Resolving Power	0.24 arcsec	0.40 arcsec
Camera	Apogee Alta F47 Mono	Atik 414EX Mono
Array size	1024 x 1024	1392 x 1040
CCD	E2V CCD47-10	Sony ICX825
Pixel size	13 x 13 $\mu\text{m}$	6.45 x 6.45 $\mu\text{m}$
ADC	16 bits	16 bits
FOV	11.7 x 11.7 arcmin	10.13 x 7.57 arcmin
Cooling	Yes, down to -50°C	Yes, down to -30°C
Plate scale	0.69 arcsec/pixel	0.44 arcsec/pixel
Software	TheSkyX	TheSkyX+Sat.Tracker

For a first order calibration, we can normalize the two optical systems via the radiance (which is proportional to the *étendue* of the systems). We can compute these using geometric optics. This will give us an absolute theoretical calibration between the two telescopes. This absolute radiometric calculation has not been applied here, but will be done in the future.

Since the detectors are different, we also need to calibrate the detectors to one another. Each detector is calibrated to itself using a set of bias frames, a set of dark frames, and a set of flat field frames (more in next epigraph).

Once we have the detectors self-calibrated between the telescopes we can use a few different methods:

- Set the exposure times to be the same. The Falcon telescope detector has a much larger well depth and dynamic range. The light curves are then normalized and just the normalized irradiance curves are compared with one another vs time.
- If the exposure time on the smaller telescope is necessarily longer, then the Falcon exposure time should be an integer fraction of the longer exposure time. This is due to the need to construct equivalent light curves via windowed averaging. So we need some number,  $n$ , of Falcon frames for each small telescope frame.
- Irradiance only curves can be compared via  $S_0$  reconstruction, however the time resolution will be at 1/3 of the effective frame rate. This is the method used in the present work.
- The light curves are calibrated to one another by using the  $S_0$  computed from the LX200 telescope and the irradiance from the FTN telescope. The calibration shown here is accomplished via a linear regression over the time points, to convert the counts in the FTN region of interest to the counts in the LX200 region of interest.

#### 4. WORKFLOW FOR ACQUISITION AND PROCESSING OF SCIENCE DATA

Astronomical images include noise coming from different sources, defined as the error in brightness levels of targets. Some noise is random and unpredictable and can be limited but not removed, whereas system noise, inherent to the imaging equipment, can be reduced, when subtracted from the raw images. Different noise sources are: readout noise, dark current, optical dust, background noise, reflections or image processing noise. The process to remove noise in the images is called data reduction.

To calibrate images from both cameras, each observation night we acquire bias, dark and flat field frames [15]. The bias frames calibrate readout noise, the dark frames calibrate thermal noise, and the flat field frames calibrate non-uniformities (e.g. detector non-uniformity and vignetting).

For correcting the different to zero counts of pixels in the cameras, “bias” images will be acquired, with zero or close to zero exposure time with the shutter closed, taken at the same temperature of the light frames. 10 bias frames are acquired, averaged and subtracted afterwards from the raw images. Dark frames are acquired with the same exposure time used in the science data. Since the polarimetric curves are obtained at 0°, 60° and 120°, we need bias, dark and flat field frames for each of these angles.

Fig. 3 shows the workflow followed in order to obtain properly calibrated science data.

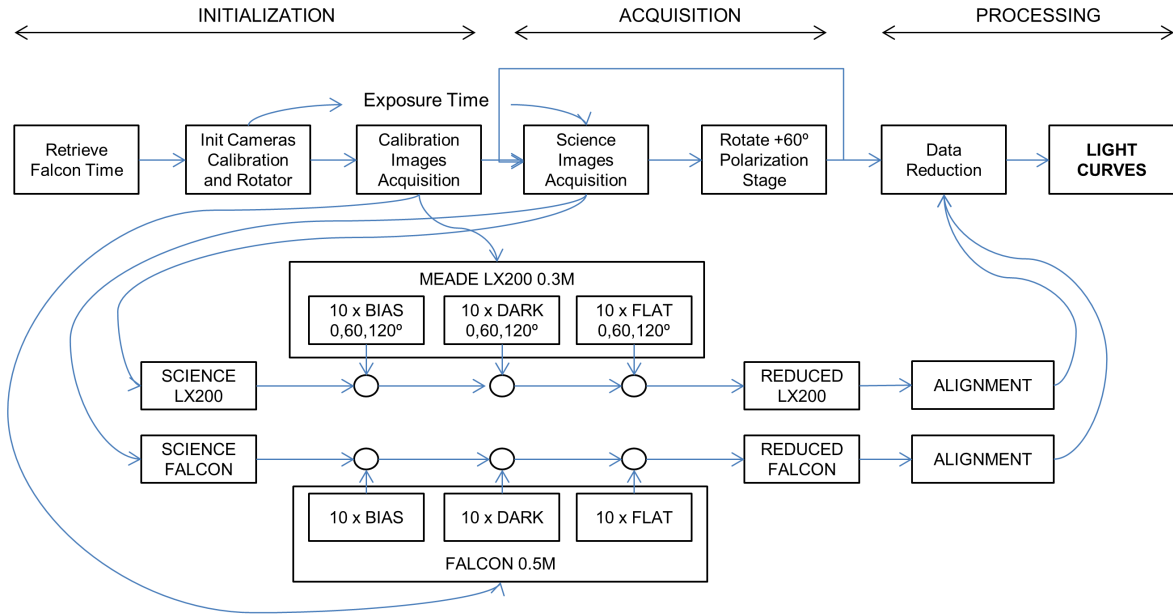


Fig. 3. Workflow to obtain calibrated science data.

The workflow includes three stages: initialization, acquisition and processing. In the initialization stage we synchronize the clocks of the control computers of each telescope, in order to minimize delays between image timestamps. We then calibrate the camera and initialise the rotation stage. The camera calibration will provide the exposure time that needs to be selected in each camera for a particular RSO in the acquisition stage. Next the bias, dark, and flat frames are acquired to calibrate each camera independently. These images are used in the processing stage.

In the acquisition stage both cameras are triggered at the same time, and the polarisation rotation stage is moved in 60° increments. When the stage reaches the angle indicated, cameras are ready to acquire the next set of images. In the final stage of processing, data reduction is applied to the science data, using the bias, dark and flat field frames obtained in the previous calibration step, and finally light curves can be computed from these images.

## 5. POLARIMETRY

The Stokes vector is commonly used to describe the polarisation of light. The vector consists of four parameters that represent a set of differential irradiance measurements,

$$\mathbf{S} = \begin{bmatrix} S_0 \\ S_1 \\ S_2 \\ S_3 \end{bmatrix} = \begin{bmatrix} I_0 + I_{90} \\ I_0 - I_{90} \\ I_{+45} - I_{-45} \\ I_R - I_L \end{bmatrix},$$

where  $s_0$  is the total irradiance,  $s_1$  is the prevalence of horizontally polarized irradiance over vertically polarized

irradiance,  $s_2$  is the prevalence of the linearly polarized irradiance at +45 over linearly polarized irradiance at -45 and  $s_3$  is the prevalence of right circularly polarized irradiance over left circularly polarized irradiance. Due to the limitations of the current state-of-the-art detectors, polarisation cannot be sensed directly and instead multiple measurements are required to reveal the underlying polarisation signature.

A single polarimeter measurement is an intensity,  $I_n = \mathbf{A}_n^T \mathbf{S}$ , where  $\mathbf{A}$  is termed the analysing vector and represents the Stokes vector of the measurement system onto which the state of polarisation is projected. If we assume that light's state of polarisation varies slower than the time required to record a series of multiple measurements, then we can effectively group the multiple measurements into a measurement matrix,

$$\mathbf{W} = [\mathbf{A}_1 \quad \mathbf{A}_2 \quad \cdots \quad \mathbf{A}_N]^T,$$

which produces a set of measurements,

$$\mathbf{I} = \begin{bmatrix} I_1 \\ I_2 \\ \vdots \\ I_N \end{bmatrix} = \mathbf{W}\mathbf{S} + \vec{n} = \begin{bmatrix} \mathbf{A}_1^T \mathbf{S} \\ \mathbf{A}_2^T \mathbf{S} \\ \vdots \\ \mathbf{A}_N^T \mathbf{S} \end{bmatrix} + \vec{n}$$

To determine the Stokes vector information, we employ the Data Reduction Method (DRM) [16],

$$\hat{\mathbf{S}} = \mathbf{W}^+ \mathbf{W}\mathbf{S} + \mathbf{W}^+ \vec{n},$$

where  $\mathbf{W}^+$  is the pseudoinverse of the measurement matrix.

As seen from Fig. 2, we oriented the polarizer in front of the LX200 telescope at three orientations: 0, 60 and 120 degrees. Given the Mueller matrix of the linear polarizer, it is easy to show that the analysing vector of the polarimeter is

$$\mathbf{A}(\theta) = \frac{1}{2} [1 \quad \cos(2\theta) \quad \sin(2\theta) \quad 0]^T,$$

which then corresponds to the following measurement matrix and its inverse,

$$\mathbf{W} = \begin{bmatrix} 0.500 & 0.500 & 0 & 0 \\ 0.500 & -0.250 & 0.433 & 0 \\ 0.500 & -0.250 & -0.433 & 0 \end{bmatrix},$$

$$\mathbf{W}^+ = \begin{bmatrix} 0.667 & 0.667 & 0.667 \\ 1.333 & -0.667 & -0.667 \\ 0 & 1.155 & -1.155 \\ 0 & 0 & 0 \end{bmatrix}.$$

Note, that because the analysing vector has  $a_3 = 0$ , the circular component of polarisation is unreconstructable.

## 6. RESULTS

Table 3 shows the three geosynchronous satellites used as targets, during three different nights. NSS-9 and OPTUS-D3 have the same configuration bus and were launched the same year. With these two satellites, we try to analyze polarisation curves of two similar objects in regard the bus and the aging of materials, at different longitudes and operated by different organizations.

OPTUS-D3 and OPTUS-C1 are two co-located Australian satellites, with different buses and launched different years. With these observations, we wanted to investigate the influence of the launch year and the bus configuration in the polarisation signatures, at the same longitude (co-location) and operated by the same organization.

Table 3. Geostationary satellites observed with their main parameters (LX: LX200 0.3m, F: Falcon Telescope 0.5m).

RSO	Launch year	Bus	Mass (launch)	Long.	Obs. day	Exp.Time (seconds)
NSS-9	2009	Star-2	2230 kg	177°	26-8-16	20(LX),10s(F)
OPTUS-D3	2009	Star-2	2500 kg	156°	27-8/4-9-16	20(L)-5(F), 15(L)-20(F)
OPTUS-C1	2003	Loral FS1300	4800 kg	155°	27-8/4-9-16	20(L)-5(F), 15(L)-20(F)

Fig. 4,5,6,7 and 8 show the  $S_0$ ,  $S_1$ ,  $S_2$ , DOLP and irradiance-only calibrated curves, for the NSS-9, OPTUS-D3 and OPTUS-C1 in different nights.

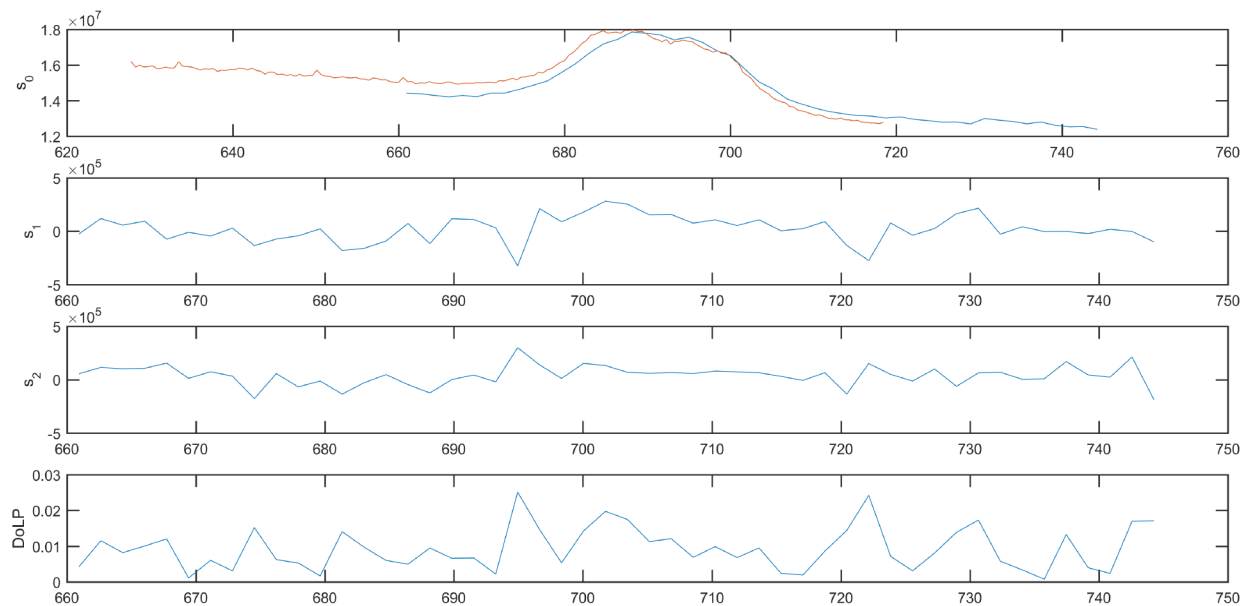


Fig. 4. NSS-9 light curves (x axis: minutes of UTC time, y axis: number of counts in ROI and DOLP). Brown curve: Irradiance only (Falcon), Blue curve (polarized light (LX200). 26-8-2016.

From fig. 4, it is observed that the reconstructed  $S_0$  curve (blue) follows closely to the irradiance-only curve (brown), which actually is expected, trend that is also observed in the rest of figures.  $S_1$ ,  $S_2$  and DOLP show low values of polarisation, and  $S_1$  and  $S_2$  show a high degree of correlation. Also the low intensity glint observed between minutes 670 and 710 in  $S_0$  doesn't seem to affect polarisation curves  $S_1$ ,  $S_2$  and DOLP.

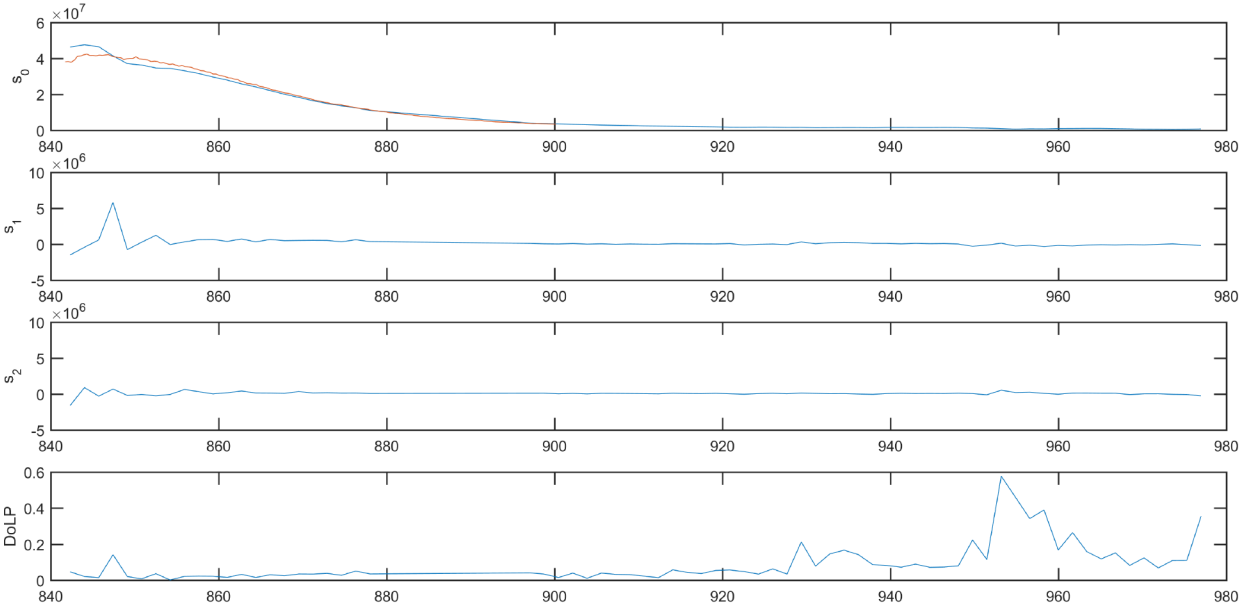


Fig. 5. OPTUS-D3 light curves (x axis: minutes of UTC time, y axis: number of counts in ROI and DOLP).  
Brown curve: Irradiance only (Falcon), Blue curve (polarized light (LX200). 27-8-2016.

From fig. 5, it is observed that during minutes 840 to 850, curves  $S_1$  and  $S_2$  show different maximum values, which suggest that during that period light coming from this particular satellite was polarized more in one direction than the other. The same trend is observed in fig. 6, corresponding to the same day and time, but for the co-located satellite, OPTUS-C1. This invalidates the assumptions that this two co-located satellites have different polarisation signatures  $S_1$  and  $S_2$ , and the cause of this behavior is probably due to other cause. Also during this period, there aren't singularity points in the  $S_0$  curve, which indicates that from polarisation curves, we obtain information not present in the irradiance only curve  $S_0$ . The main differences between fig. 5 and 6 are the different slopes in  $S_0$  curves.

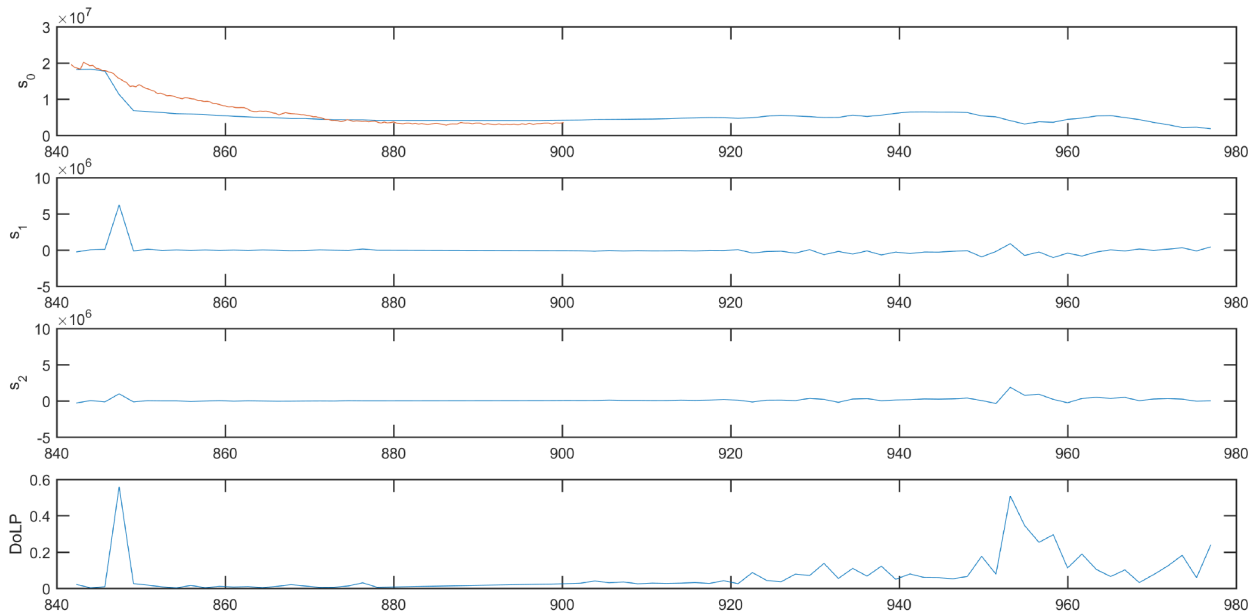


Fig. 6. OPTUS-C1 light curves (x axis: minutes of UTC time, y axis: number of counts in ROI and DOLP).  
Brown curve: Irradiance only (Falcon), Blue curve (polarized light (LX200). 27-8-2016.

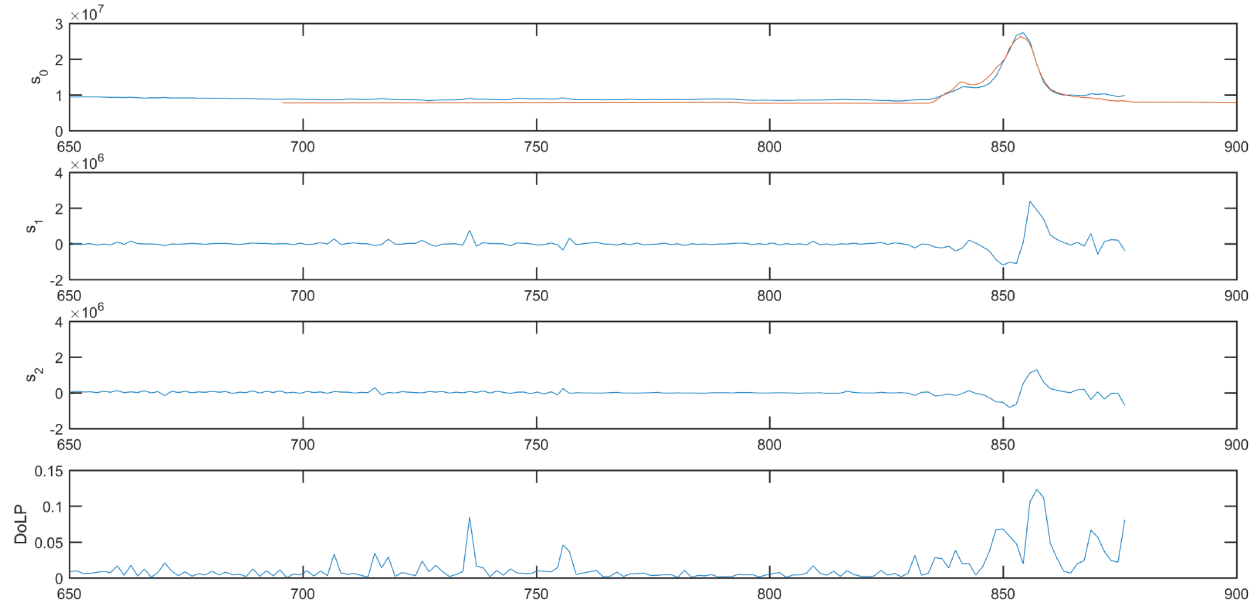


Fig. 7. OPTUS-D3 light curves (x axis: minutes of UTC time, y axis: number of counts in ROI and DoLP).  
Brown curve: Irradiance only (Falcon), Blue curve (polarized light (LX200). 4-9-2016.

Fig. 7 shows light curve of OPTUS-D3 a different night. Curves  $S_1$  and  $S_2$  show correlation and their values are close to zero. The exception to this trend is when the glint occurred, between minutes 840 and 860, which can be appreciated clearly in  $S_0$ . There are relative smaller values in the polarisation curves  $S_1$  and  $S_2$ , when the glint occurred, which suggest that we should use higher exposure times in LX200 telescope, in order to get higher S/N ratio in the measured number of counts.

Fig. 8 also shows OPTUS-C1 night of 4-9-2016. As in the case of the OPTUS-D3 light curve, it is noted the difference magnitude between curves  $S_1$  and  $S_2$ , when another glint occurred around minute 840. Degree of polarisation shows closed to zero values.

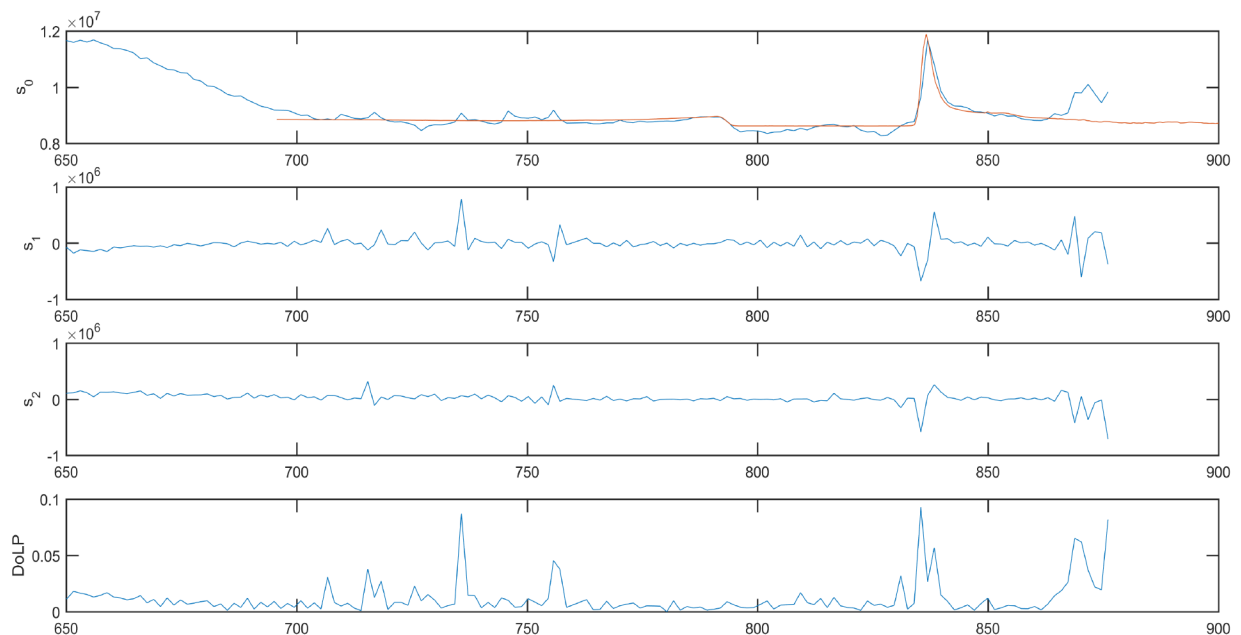


Fig. 8. OPTUS-D3 light curves (x axis: minutes of UTC time, y axis: number of counts in ROI and DoLP).  
Brown curve: Irradiance only (Falcon), Blue curve (polarized light (LX200). 4-9-2016.

## 7. CONCLUSIONS

UNSW Canberra Space Group has expanded his current capabilities with synchronized optical sensors aiming to the geostationary belt, using small aperture (less than 0.5 m) telescopes, and using a novel approach to compare polarisation curves in one telescope, with intensity only curves in another.

A first set of experiments to obtain light curves of polarisation signatures coming from single and clusters geostationary satellites has been accomplished. These results are a first step to the characterization of geosynchronous satellites through polarimetry, and from the results some differences between curves can be appreciated, namely: different intensities magnitudes between curves  $S_1$  and  $S_2$ , different slopes between intensity only signatures obtained with Falcon telescope and reconstructed  $S_0$  curve from polarimetry, and increasing magnitude of polarisation curves when glints occur.

At this stage, with the experiments accomplished thus far, it is difficult to extract useful information from the polarisation light curves, but lessons learned in this first stage are guiding us for next step of this project, considering the next topics:

- Longer runs of experimental measurements need to be performed with different satellites and types of buses, in order to evaluate a wider range of phase angles, to associate patterns to polarisation signatures as a function of different buses, solar panel configurations and possible aging of materials
- Evaluation of complete Stokes parameter measurements.
- Increase the speed of the acquisition stage, and therefore the light curves resolution, in order to detect small changes in polarisation signatures that right now could be undetected.

## 8. ACKNOWLEDGEMENTS

We would like to thank the USAFA for the donation of equipment and participation in the Falcon Telescope Network.

## 9. REFERENCES

1. Larson, W.J. and Wertz, J.L., *Space Mission Analysis and Design*, 3<sup>rd</sup> ed, Microcosm Press, 2006.
2. M. Hart, R. Rast, S. Jefferies, and D. Hope, *Resolved observations of geostationary satellites from the 6.5 m MMT*, AMOS Conference, Hawaii, US, 2015.
3. D. Mozurkewich, H. R. Schmitt, and J. T. Armstrong, *Fundamental limitations for imaging GEO satellites*, AMOS Conference, Hawaii, US, 2015.
4. R. Schmitt et al, *Simulated optical interferometric observations of geostationary satellites*, SPIE 2011.
5. T. E. Payne, P. J. Castro, and S. A. Gregory, *Satellite Photometric Error Determination*, AMOS Conference, Hawaii, US, 2015.
6. C. R. Binz, M. A. Davis, B. E. Kelm, and C. I. Moore, *Optical Survey of the Tumble Rates of Retired GEO Satellites*, AMOS Conference, Hawaii, US, 2014.
7. Ryan M. Tucker, E. M. Weld, F.K. Chun, and R.D. Tippetts, *Spectral Measurements of Geosynchronous Satellites During Glint Season*, AMOS Conference, Hawaii, US, 2015.
8. Scott Tyo J., Goldstein L., Chenaut D.B., Shaw J.A., *Review of passive imaging polarimetry for remote sensing applications*, Applied Optics, Vol. 45, No. 22, August 2006.
9. Stryjewski J. et al., *Real Time Polarization Light Curves for Space Debris and Satellites*, AMOS Conference, Hawaii, US, 2010.
10. Pasqual M.C., Kahoi K.L., Hines E.L., *Active Polarimetry for Orbital Debris Identification*, AMOS Conference 2015.
11. A. Speicher, M. Matin, R. D. Tippetts, and F. K. Chun, *Calibration of a system to collect visible-light polarization data for classification of geosynchronous satellites*, Proceedings of SPIE, vol. 9223, p. 922308, 2014.

12. A. Speicher, M. Matin, R.D. Tippetts, F.K. Chun and D. Strong, *Results from an experiment that collected visible-light polarization data using unresolved imagery for classification of geosynchronous satellites*, Proceedings, SPIE, vol. 9460, p. 946006, 2015.
13. Israel J. Vaughn, Brian G. Hoover, and J. Scott Tyo, *Classification using active polarimetry*, Proceedings SPIE, vol. 8364, 83640S, June 11, 2012.
14. François Goudail, *Optimization of the contrast in active Stokes images*, Opt. Lett. 34, 121-123, 2009.
15. Software Bisque Inc., *TheSkyX Professional and Serious Astronomer Edition User Guide*. Rev. 3.5, 2014.
16. R. A. Chipman, *Handbook of Optics* (McGraw Hill, 2009), vol. 1, chap. 15, pp. 15.1-15.41, 3rd ed.